LA-UR- 11-05857

Approved for public release;
distribution is unlimited.

Title: FY11 Campaign 1 pRad RMI activities quick-look report

Author(s):
W. T. Buttler, P-23
D. M. Oro, P-23
F. G. Mariam, P-25
C. Morris, P-25
J. B. Stone, P23
D. Tupa, P-25

Intended for: C1 Program Manager

Los Alamos
NATIONAL LABORATORY
EST. 1943

Los Alamos National Laboratory, an affirmative action/equal opportunity employer, is operated by the Los Alamos National Security, LLC for the National Nuclear Security Administration of the U.S. Department of Energy under contract DE-AC52-06NA25396. By acceptance of this article, the publisher recognizes that the U.S. Government retains a nonexclusive, royalty-free license to publish or reproduce the published form of this contribution, or to allow others to do so, for U.S. Government purposes. Los Alamos National Laboratory requests that the publisher identify this article as work performed under the auspices of the U.S. Department of Energy. Los Alamos National Laboratory strongly supports academic freedom and a researcher's right to publish; as an institution, however, the Laboratory does not endorse the viewpoint of a publication or guarantee its technical correctness.

Form 836 (7/06)

FY11 Campaign 1 pRad RMI activities quick-look report

W. T. Buttler, D. M. Oró, F. G. Marriam, C. Morris, J. B. Stone, and D. Tupa
Los Alamos National Laboratory, Physics, Los Alamos, NM 87544, USA

In FY11 we fielded four pRad experiments with 76 mm diameter HE lenses, with three of the four experiments returning data. The first experiment was a repeat of an FY10 Cu experiment that fielded a 10 mm thick PBX 9501 booster, where we narrowed our amplitude phase space while maintaining a perturbation wavelength of $\lambda = 550$ μm; the experimental objective is to validate and quantify with reduced uncertainty the FY10 Cu yield at high strain ($< 700\%$) and high strain rates ($> 10^7$/s). The second experiment was a two-shockwave experiment with Cu that fielded two PBX 9501 boosters and a Ta tamper, but no data were returned; the wavelengths were again $\lambda = 550$ μm. The third experiment was a single shockwave Sn transport experiment into 2.5 Atm. Ne, where we fielded a 16 mm thick calcitol booster to drive a thick Sn target, and where we varied the wavelengths such that $450 \leq \lambda \leq 900$ μm, and the fourth experiment was a repeat of the Cu two-shockwave experiment.

I. INTRODUCTION

Los Alamos National Laboratory (LANL) is actively engaged in the development and implementation of ejecta source and transport models. The effort supports theory and model development with experimental flyer-plate and high-explosive (HE) driven ejecta source and transport measurements from machine roughened Sn surfaces (see Buttler et al. [1, 2], Buttler & Zellner [3], Vogan et al. [4], Zellner et al. [5, 6, 7, 8], Zellner & Buttler [9]), to measurements presented here from surfaces with larger scale perturbations that permit the study of the physics of ejecta production with dynamic penetrating proton radiography (pRad). Our FY11 C1 efforts support these goals by application of our C1 FY10 data to parallel C2 ejecta model development. Our FY11 C1 activities also made use of a two-shockwave experimental tool developed under C2. We also repeated one FY10 Cu experiment that focused on determining the strength of Cu at zero pressure and high strains and strain rates, and we fielded one Sn experiment into 2.5 Atm. Ne. This transport experiment is meant to be paired with an otherwise identical Sn shot into 10 Atm. He, but that experiment has slipped into FY12.

II. EJECTA MODEL FROM FY10 PRAD RMI DATA

There are at least two approaches to modeling ejecta dynamics. One technique measures total mass-velocity distributions from a variety of surface finishes across a spectrum of shock breakout pressures, P_{SB}. Those source measurements can be inserted into a hydrodynamic-code that adds the measured source into the hydrodynamics when some critical condition is exceeded. Another approach is to characterize materials according to their dynamic material properties and sensitivities to the initial drive conditions. Assuming a robust physics based model can be developed for a spectrum of interesting metals, then the parameter space of variables can be reduced. At a minimum, such a model will accurately predict the total ejected mass and its velocity distribution based on the material and the geometry of the surface perturbations. It is this approach we are pursuing.

Our recent RM experiments at LANL explore ejecta physics around three features: total mass ejected, ejecta mass velocity distributions, and driving conditions under which ejecta do or do not form. The first two criteria for mass ejected from shocked metals at the metal-vacuum interface link to a liquid (*mostly* strength-less) RM instability model, while the final criterion links plastic unstable flow to materials with strength.

Considering the first two criteria, in the $A = -1$ limit for metals that liquefy on shock or shock release, for the situation that a shockwave is driven through a metal into sinusoidal perturbations at the metal-vacuum interface. When the shockwave arrives at the metal-vacuum interface it will first release to zero-pressure at the perturbation minimum and then reflect back into the metal as a rarefaction wave. A brief time later the shockwave releases to zero-pressure at the perturbation maximum, also reflecting back into the metal as a rarefaction wave. Under these conditions, strains produced by the shockwaves interacting with the perturbations and the vacuum interface causes the perturbation minimums to compress, invert, and then grow in tension as RM instabilities (spikes) into vacuum. Because the compressed RM spikes grow quickly relative to the initial perturbation maximums, the perturbation maximums invert and form bubbles that unstably grow into the metal causing metal to flow into the spikes to support the spike growth. In this picture, bubbles and spikes refer to peak penetration depths on the two opposite sides of the "free-surface," which is nominally defined as the initial zero amplitude of the sinusoidal perturbations, e.g., the initial surface sinusoidal perturbation can be defined as $\eta(x) = \eta_0 \sin(kx)$, where the wavenumber $k = 2\pi/\lambda$, λ is the

perturbation wavelength, x is the planar (xz) dimension parallel to the "free-surface" and incident shockwave, and η_0 is the initial perturbation amplitude oriented parallel to the vertical dimension (y-axis) orthogonal to the xz-plane. In this two-dimensional geometry the literature usually takes $\eta(x,t)$ positive into the metal, and $-\eta(x,t)$ into the vacuum. With this definition, we define $\dot{\eta}^{b,s}(x,t)$ as the velocities of the bubbles (spikes) relative to the free surface velocity u_{fs} – in the laboratory frame we directly measure with laser Doppler velocimetry (LDV) u_{fs}, $u^b_\infty = u_{fs} - \dot{\eta}^b$, and $u^s_\infty = u_{fs} + |\dot{\eta}^s|$, e.g., see [10–14].

We shall use the linear theory developed in [15] to describe the extremely short, early time evolution of the perturbations as the perturbations compress when they pass through zero during the inversion process. For the subsequent period of substantial growth (more than thirty fold) we use a nonlinear model developed in [16] to describe the evolution of bubbles and spikes relative to the free surface.

Setting $g = \eta_0 k = 0$ in Eq. 5a in [16], gives

$$\frac{\dot{\eta}}{\dot{\eta}_0} = \frac{\mathcal{Y}_0}{\mathcal{Y}} = \sqrt{\frac{3}{2}}\frac{1}{\mathcal{Y}} = \sqrt{\frac{3}{2}}\frac{1}{\sqrt{e^{3\eta k} + 1/2}}, \tag{1}$$

where $\mathcal{Y}^2 = e^{3\eta k} + 1/2$. This equation applies to both bubbles and spikes, as pointed out by Zhang [17], provided we take η and $\dot{\eta}$ positive (negative) for bubbles (spikes). Equation 1 relates the bubble or spike velocity $\dot{\eta}^{b,s}$ to its amplitude $\eta^{b,s}$, and its initial growth rate $\dot{\eta}_0$, which we now describe.

Integrating Eq. 1 gives

$$\begin{aligned} \dot{\eta}_0 k\, t &= \frac{2\sqrt{2}}{3\sqrt{3}}\mathcal{Y} - \frac{2}{3} + \frac{1}{3\sqrt{3}}\ln\left[\frac{(\sqrt{3}+1)(\sqrt{2}\mathcal{Y}-1)}{(\sqrt{3}-1)(\sqrt{2}\mathcal{Y}+1)}\right] \\ &= \frac{2\sqrt{2}}{3\sqrt{3}}\mathcal{Y} - \frac{2}{3} + \frac{\eta k}{\sqrt{3}} + \frac{1}{3\sqrt{3}}\ln\left[\frac{\sqrt{3}+1}{(\sqrt{3}-1)(\sqrt{2}\mathcal{Y}+1)^2}\right], \end{aligned} \tag{2}$$

which is equivalent to Eq. 11 in [16] with $\eta_0 k = 0$, and Eq. 36 in [18].

The asymptotic spike velocity can be approximated from either Eq. 1 or 2 by evaluating both equations as $\eta^s \to -\infty$. For Eq. 2, the terms must be rearranged, but from Eq. 1 we find

$$\lim_{\eta \to -\infty} \dot{\eta}(\eta) = \sqrt{3}\dot{\eta}^s_0, \tag{3}$$

which is the maximum velocity attainable by the spikes in this model.

An approximation to the bubble velocity in Eq. 1 is given as Eq. 17 in [16]

$$\begin{aligned} \dot{\eta}^b_t &= \frac{2\dot{\eta}^b_0}{2 + 3\dot{\eta}^b_0 k t} \\ \Rightarrow \dot{\eta}^b_\infty &\equiv \lim_{t\to\infty} \dot{\eta}^b_t = \frac{2}{3kt}. \end{aligned} \tag{4}$$

The asymptotic limit applies at very late times and is independent of the initial perturbation amplitudes.

Equations 1 to 4 require the initial growth rates $\dot{\eta}^{b,s}_0$. For shockwave driven incompressible linear instability growth ($\eta_0 k \ll 1$)

$$\dot{\eta}^b_0 = -\dot{\eta}^s_0 = \eta_0 k u_{fs}, \tag{5}$$

as shown by Richtmyer [15]. This result is modified by two effects: compressibility and nonlinearity. Richtmyer showed that to account for compressibility one should use not the preshock amplitude η_0 but the postshock, compressed amplitude $\eta_0(1 - u_{fs}/u_{sh})$, where u_{sh} is the shockwave speed in the metal caused by the loading stress P_{SB} just prior to the arrival of the shockwave at the free-surface. While Richtmyer investigated the case of a shockwave moving from a low- to a high-density fluid ($A = 1$), for the opposite case ($A = -1$) Meyer & Blewett [19] found that using the average of the preshock and postshock amplitudes gave better agreement with direct numerical simulations. Hence we use

$$F_{cmp} = 1 - \frac{u_{fs}}{2u_{sh}} \tag{6}$$

as the compression factor. These prescriptions were developed for linear amplitudes and therefore the compression factor is the same for both bubbles and spikes, i.e., $F^b_{cmp} = F^s_{cmp} = F_{cmp}$.

In the nonlinear regime ($\eta_0 k \gtrsim 1$) a nonlinearity factor F_{nl} differentiates between bubbles and spikes. Velikovich & Dimonte [20] addressed the nonlinear regime with a perturbation model and a series of simulations of bubble and spike growth. Later, [21] provided a nonlinear factor as a fit to the spike simulations in [20]:

$$F_{nl}^{s} = \frac{1}{1 + (\frac{\eta_0 k}{2})^2}. \tag{7}$$

A similar fit to the bubble amplitudes gives a nonlinear bubble factor:

$$F_{nl}^{b} = \frac{1}{1 + \frac{\eta_0 k}{6}}. \tag{8}$$

Assuming that compressible and nonlinear effects act independently we obtain

$$|\dot{\eta}_0^{b,s}| = F_{cmp} F_{nl}^{b,s} |\eta_0 k u_{fs}|. \tag{9}$$

The third criterion we explore evaluates whether ejecta formation is more fundamental than a simple link to the material phase at the time of shock or shock release at the metal-vacuum interface, i.e., are the criteria of ejecta formation fundamentally linked to basic material properties, such as material strength at the strains and strain rates in the material as experienced in the interaction of shock induced stresses and the perturbation geometry. If this last hypothesis is correct, then it is possible to form ejecta even when the material is solid on shock and shock release. This hypothesis centers on an interesting result in Piriz, et al. [22]. In that work, they develop a model to evaluate the elastic-perfectly plastic yield Y of a material. They do this by examining unstable growth of perturbations when $A = 1$, which is different than our physics regime with $A = -1$. Their result relates Y to the amplitude of the spikes that begin to grow plastically, but then the plastic growth arrests prior to spike breakup or material failure. For example, along these lines, in Eq. 39 in Piriz, et al. [22] they find:

$$\xi_m - \xi_0 = 0.29 \frac{\rho \dot{\xi}_0^2}{kY}, \tag{10}$$

where ξ_m is the height the spike reaches after inversion, growth and arrest, $\dot{\xi}_0 \equiv k\xi_i u_p$, u_p is particle velocity in the shocked material (when $A = -1$, $u_p \mapsto u_{fs}$), and $\xi \equiv \eta$ in our coordinate system definition but $\xi_0 > \eta_0$.

The equivalent value to η_0 in our work is ξ_i in Piriz, et al. [22]. The difference between ξ_0 and ξ_i (η_0) relates the difference between the elastic regime of the spike growth, as compared with plastic regime of spike growth. For our situation, the time over which elastic behavior during the unstable spike growth is important is small relative to the time over which plastic behavior is important. This is summarized in [22] by comparing Y with the material shear modulus $G = \rho c_s^2$. Essentially, $\xi_0 \approx \xi_i$ when $Y/(k\xi_i G) \ll 1$. For our situation, for the Cu and Sn experiments presented later, Y is of $O(0.5$ GPa), and $G_{Cu} \approx 48$ GPa (Cu), and $G_{Sn} \approx 18$ GPa (Sn). Therefore, $\xi_0 \approx \xi_i = \eta_0$ during the plastic unstable growth of the spikes, implying Eq. 39 in [22] is

$$(\eta_\infty^s - \eta_0)k \approx \mu \eta_0 \frac{\rho_0 (\eta_0 k u_{fs})^2}{Y} \approx 0.29 \eta_0 \frac{\rho_0 (\eta_0 k u_{fs})^2}{Y}, \tag{11}$$

where $\mu = 0.29$ is a parameter fit by simulation, ρ_0 is the material density at zero pressure, and where Y must be the mean flow stress of the material at high strains and high strain rates – not the elastic-perfectly plastic yield assumed in Piriz, et al. [22], Piriz, Lopez-Cela & Tahir [23]. We explore this property in shock stress regimes where the material is solid on shock and release, with $A = -1$, in contrast with the Piriz study where $A \approx 1$.

The simulations in Piriz, et al. [22] and [23] used to fit the parameter $\mu = 0.29$ were evaluated under an assumption of incompressible flow for $A = 1$ ([22]); the authors note that their simulations were accomplished with a Mie-Grüneisen equation of state (EOS), an EOS that allows for compressibility. Regrettably the authors do not say what they used for Grüneisen-γ, and it is possible they chose Grüneisen-γ such that the EOS was "stiff." But if their choice for Grüneisenγ allowed for compressibility – as it should, then compressibility is absorbed in $\mu = 0.29$. If true, then this implies that a first order approximation of Eq. 11 for $A = -1$ scales μ to μ'

$$\mu' \approx \mu \times \left[\left(1 - \frac{u_{fs}}{2u_{sh}}\right) \Big/ \left(1 - \frac{u_{fs}}{u_{sh}}\right) \right]^2. \tag{12}$$

If similar simulations as those carried out in [22] are performed for our $A = -1$ physics, μ' might be rather different than the simple scaling implied in 12; nevertheless the compression factors for the two regimes scale as presented.

There are other key differences between the model in Piriz, et al. [22] and our experiments. For example, their model assumes that $\dot{\eta}^s \equiv \dot{\eta}^b$, which is true for their $A = 1$ study; our $A = -1$ situation releases to zero pressure and the spike and bubble velocities and heights are quite different from one another. Regardless theirs is a relevant idea and approach, and it was the motivation behind our interest in solid material RM studies. The experimental results support the motivation.

The model described by Eqs. 1 to 9 is under consideration for publication in the Journal of Fluid Mechanics [24], and will also appear in abbreviated form in [25]. The model was validated with FY10 C1 pRad RMI data. The strength model described by Eqs. 10 to 12 are also included in [24], and is also the subject of a manuscript submitted to Physical Review Letters [26].

III. EXPERIMENTAL APPROACH

The path by which we arrived at our present experimental approaches to explore the physics described by Eqs. 1 to 11 began with small scale HE and flyer-plate experiments on roughened surfaces [4, 5]. From those studies it was concluded that the geometries of most interest centered on one-dimensional (1D) HE driven experiments. The 1D approach led naturally to use of HE lenses combined with boosters to smooth out the drive as the shockwave releases to zero pressure as it arrives at the vacuum-metal interface. Also, because of our successes with the smaller scale experimental studies, we began pRad work with larger scale perturbations that were imageable at the pRad facility. Our designs now are mature, utilizing momentum trapping concepts [27, 28], large 76 mm diameter HE lenses, and we have maximized tuned our packages wavelengths and amplitudes to maximize our data return with the $\times 3$ magnification offered by the pRad facility.

Our FY11 campaign explored transport of ejecta with a Sn package by observation of RM unstable growth into 2.5 Atm. Ne, Cu strength at high strains and strain rates into vacuum, and the effect of a second shock on RM unstable growth into vacuum as well. All experiments utilized a P076 HE lens (76 mm diameter lens), and 76 mm diameter HE boosters. Depending on the experiment, the HE booster thickness was varied, and the HE booster and booster material was varied.

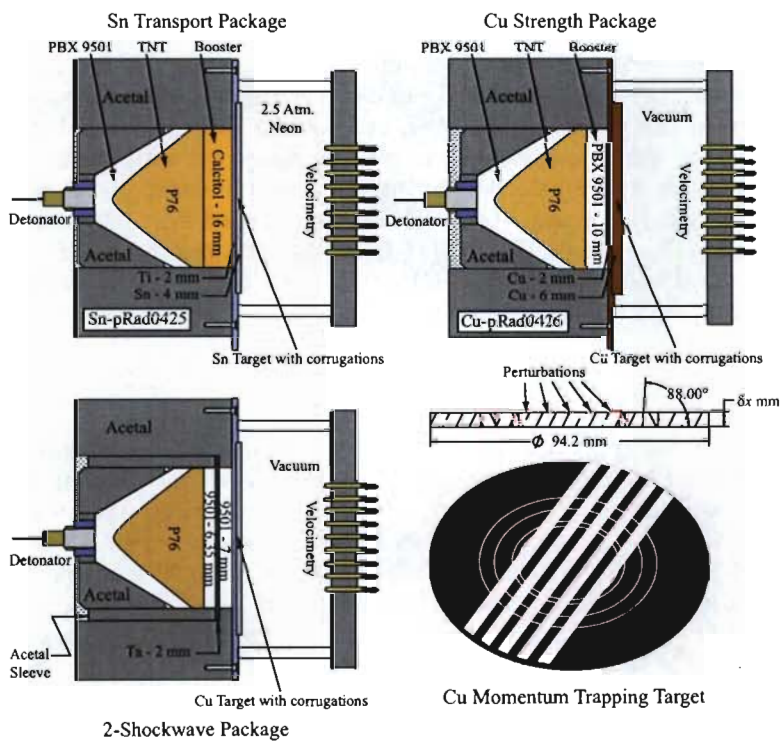

FIG. 1: pRad RM experimental package geometries encase in acetal plastic a 76 mm diameter plane-wave HE lens used to uniformly detonate a HE booster cylinder in contact with a buffer plate. The target design incorporates momentum trapping concepts [27, 28], as illustrated on the lower right together with the target perturbation schemes. Each corrugation band was up to seven wavelengths wide and separated by flat regions that were ≈ 5 mm wide. Over each corrugation band and intervening flat region was positioned a velocimetry probe used to measure jump times and velocity histories.

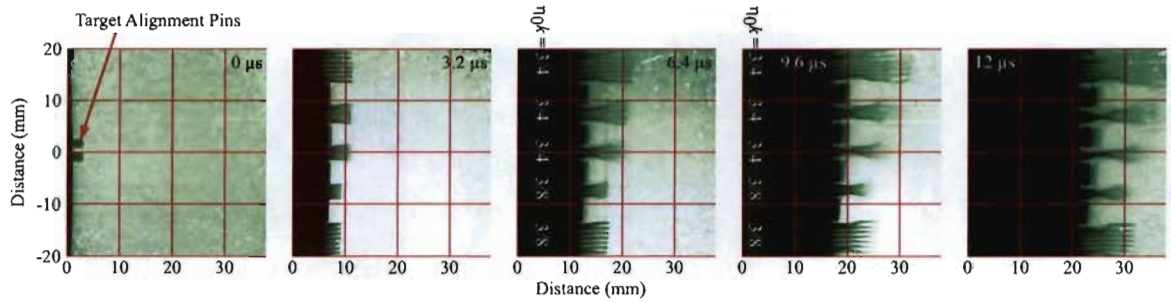

FIG. 2: Selected FY11 Sn transport pRad images. The target alignment pins are seen the left-most image. It is seen that the three $\eta_0 k = 3/4$ RM spike velocities are similar at early times, but the smaller wavelength RM spikes appear to be breaking up more quickly, as evidences in the apparent deceleration of the spikes.

Each experiment – Sn and Cu – had 5 perturbation regions on the surface separated by diamond turned regions. Above each perturbation region was positioned laser Doppler velocimetry (LDV), and LDV was positioned above the diamond turned finish flat regions as well. The velocimetry from the flat regions gives the jump velocity at the vacuum (or Ne gas) metal interface. This jump velocity is used to estimate the loading pressure P_{SB} as the shockwave releases at the vacuum metal interface (relative to the shockwave pressure in the metal 2.5 atm. Ne, or any gas, is essentially vacuum as well). The proton radiographs shows where and how the ejecta (RM unstable growth) evolves in vacuum and gas, and offers the possibility to evaluate the Cu and Sn densities. The basic FY11 RM packages are shown in Fig. 1.

A. Sn transport experiments

The Sn package fielded a 16 mm tall Calcitol booster of diameter 76 mm. We fielded a Sn package in FY10 with this booster geometry with the perturbation wavelengths fixed at $\lambda = 550$ μm, but without momentum trapping, and the Sn was observed to reach a peak stress of $P_{SB} \approx 26$ GPa; this is the same P_{SB} observed in FY11.

For this FY11 experiment the perturbations were machined so that the wavenumber $k = 2\pi/\lambda$ and amplitude η_0 products were $\eta_0 k \in \{3/8, 3/8, 3/4, 3/4\}$. In addition, for this Sn experiment the wavelengths were varied, in the same

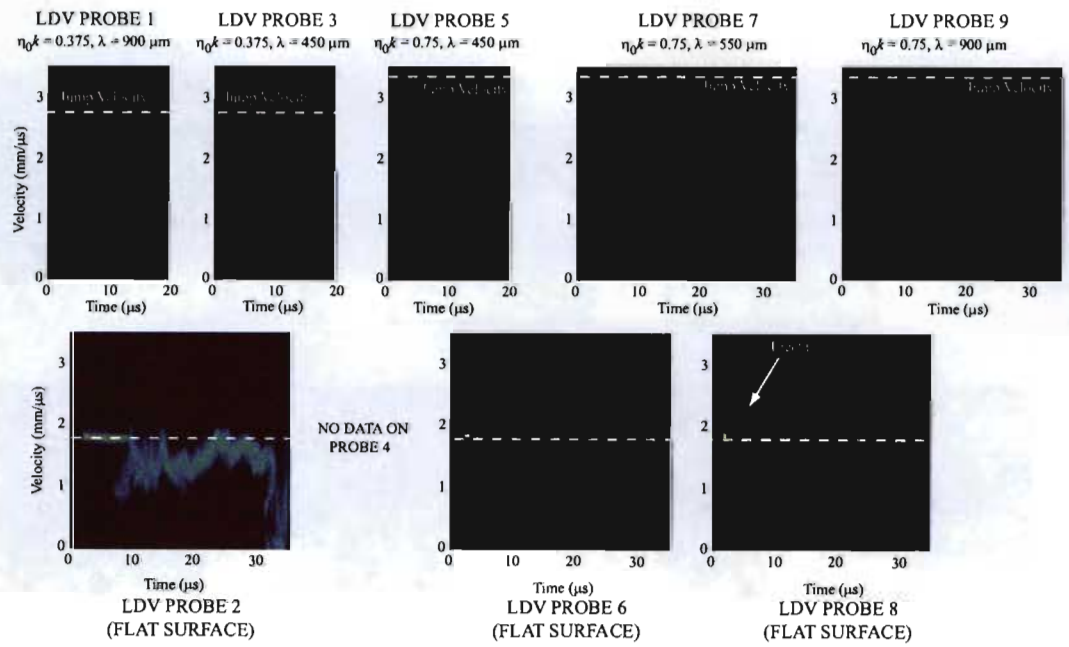

FIG. 3: FY11 Sn-transport velocimetry. Seen in the data are that the RM spikes persist longer with the larger wavelength for each $\eta_0 k$. We define persistence to be the time at which the leading edge of the spike tip begins to roll over.

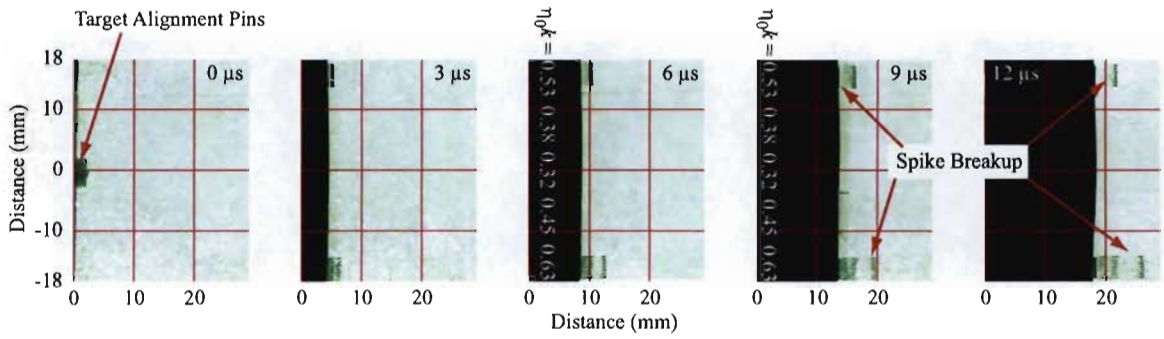

FIG. 4: Selected FY11 Cu strength pRad images. As noted in the text, some of the perturbation regions are expected to begin to grow and the growth quickly arrest – due to material strength. Some perturbation regions will be seen to grow plastically and then breakup. The images reflect this prediction, and the velocimetry supports the conclusion.

ordering as above, to be $\lambda \in \{900, 450, 450, 550, 900\}$ μm.

The larger RM spike diameters should penetrate deeper into the Ne gas over a longer time than the smaller RM spike diameters (spike diameter should link to the initial wavelength), because it is thought that the particle/ejecta sizes will scale with the wavelength, i.e., larger wavelengths give larger ejecta particle sizes, and they would thus breakup more slowly than the smaller wavelength perturbation regions. A longer term goal is to pair this experiment with another Sn experiment with otherwise identical parameters into 10 Atm. He to look for viscous effects on particle breakup. The density of 10 Atm. He is the same as 2.5 Atm. Ne. Thus, differences in particle breakup would link to viscous effects. The companion experiment will be fielded in FY12. Selected images from the FY11 experiments are shown in Fig. 2, and the Sn transport velocimetry is shown in Fig. 3

B. Cu strength experiment

This Cu package fielded a 10 mm tall PBX 9501 booster of diameter 76 mm. This was a repeat of an FY10 experiment that was used to estimate the strength of Cu at highs strains (> 700%) and high strain rates (> 10^7/s). The goal of this experiment is to provide data to reduce the uncertainty of the FY10 Cu yield strength estimate, which was determined to be as high as $Y \lesssim 5.2$ kbar. This result was compared with a PTW calculation that found $Y \approx 5.7$ kbar at the experimental strains and strain rates over the duration of the experiment. While the comparison

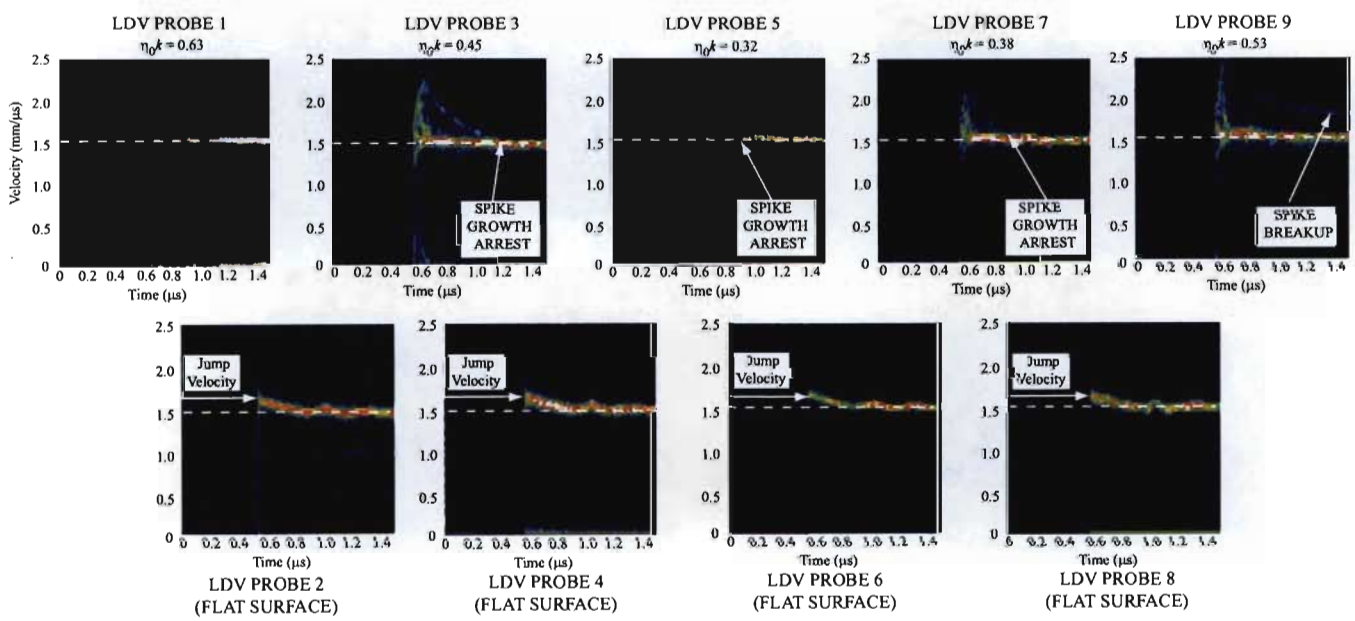

FIG. 5: FY11 Cu-strength velocimetry. Discussion is within the text.

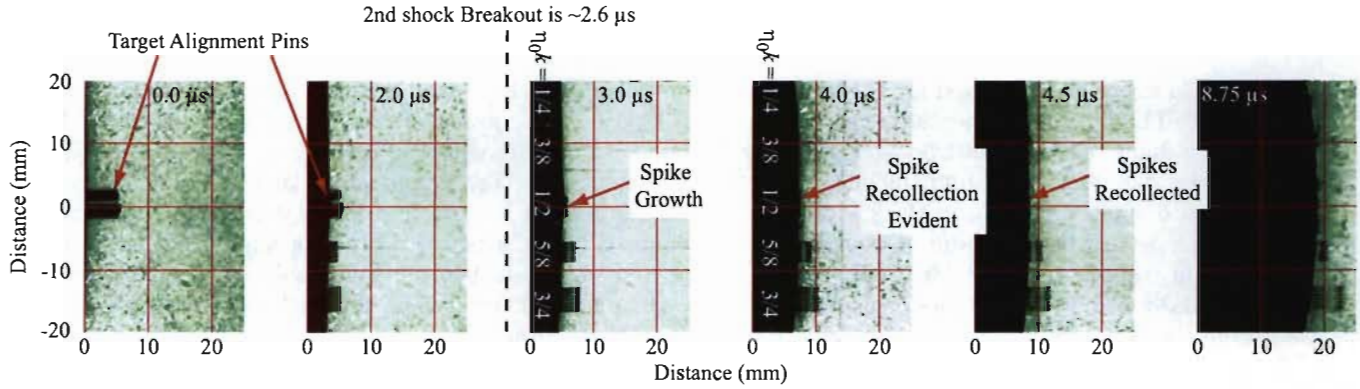

FIG. 6: Selected pRad images from the uniaxial strain two-shockwave experiment. Similar to the strength experiment, some spikes grow and then the growth is arrested. Some spikes grow and breakup, and the second shockwave begins to recollect the broken up spikes. See velocimetry and text for more details.

with PTW is encouraging, it must be noted that PTW is not benchmarked at these strains and strain rates. In fact, the PTW approximations are not validated in this regime and it is of interest to have data in this regime on a number of metals to develop a high strain and high strain rate model in the continuum. This type of experiment may be our only tool to estimate material yield strength at these strains and strain rates; beyond $\varepsilon > 10^9$/s phonon modes are excited, according to theory, implying that the material is in a quantum regime. Figure 4 presents selected pRad Cu strength data.

If Eq. 11 captures the physics relevant to unstable RM growth in solids with $A = -1$, then the dynamics predicted for a target that is solid on release, assuming the perturbation wavenumbers are well chosen, are that at least one perturbation region will grow without bound, another perturbation region will not grow at all (its velocimetry would be indistinguishable from the free surface velocity u_{fs}), and that at least one of the remaining perturbation regions will present with initial plastic RM growth that quickly arrests; these are the dynamics observed in the Cu experiment (see Fig. 4). The velocimetry for the Cu-strength experiment is presented in Fig. 5. The lower 4 images show the velocity of the diamond turned flat regions, where the jump velocity is nominally seen to be $u_{jump} \approx 1.65$ mm/μs, which correlates to $P_{SM} \approx 38$ GPa. The upper 5 images show the velocity of the perturbation regions. Probe 1 had a low data return, but the remaining probes show spike growth and arrest (probes 3, 5, and 7), and probe 9 presents perturbations that plastically grow, release down to a lower velocity, and breakup prior to full arrest.

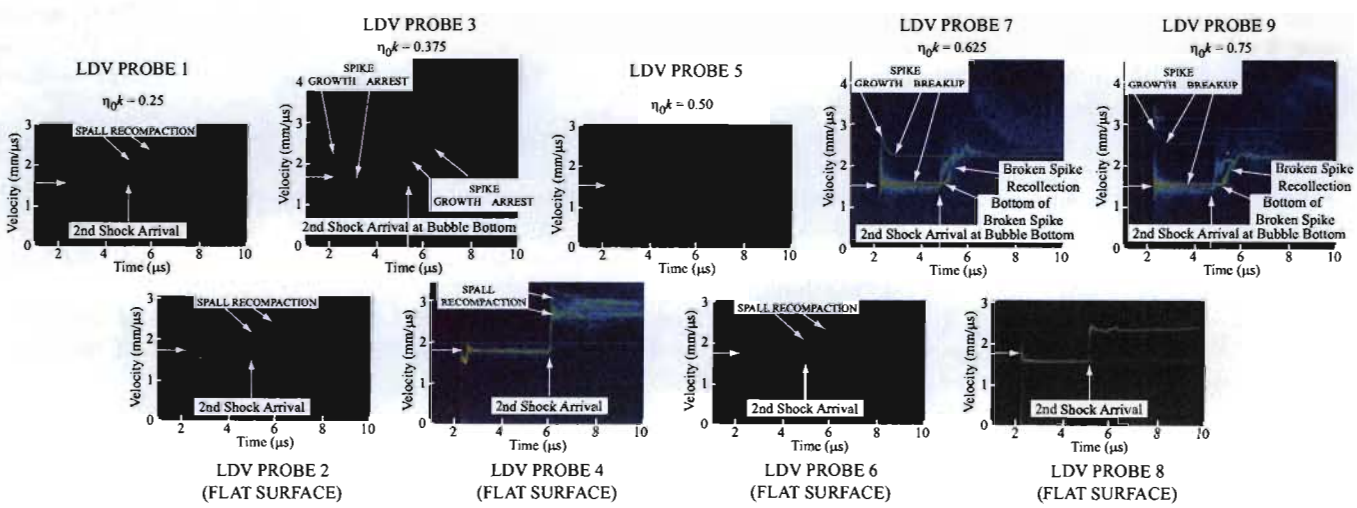

FIG. 7: Cu 2-shockwave velocimetry. Probes 1 and 5 had low data return, but probes 7 and 9 show spike growth and breakup, and spike recollection. Probes 2, 4, 6, and 8 show the first and second shock jump velocities ($u_{1st} \approx 1.8$ mm/μs, and $u_{2nd} \approx 0.9$ mm/μs), the time interval (≈ 2.6 μs), and recompaction of the spalled Cu.

C. First experimental two-shockwave data in uniaxial strain

The third Cu experiment utilized for the first time a two-shockwave drive that was developed under campaign two activities in FY11. This experimental geometry is seen in Fig. 1 on the lower left, and it utilizes a P076 HE lens to drive a 76 mm diameter PBX 9501 booster of height 6.35 mm. In contact with the PBX booster is a piece of Ta that is about 85 mm diameter and 2 mm thickness. On the other side of the Ta, in contact, is another PBX 9501 booster that is 76 mm diameter and 7 mm thick. In contact with this second booster is a Cu plate on which the target is assembled with 4 Cu rings enclosing a central Cu disk mounted to a Cu plate; this 4-ring and 1-disk assembly was the momentum trapping concept for the experiment. The assembly was then machined to a diamond turned finish and 5 sinusoidal perturbation regions were machined onto the diamond turn finish, the back-side of the target which is away from the HE. Figure 6 presents selected Cu two-shockwave pRad images.

LDV was positioned above the perturbation regions and the intervening flat regions. The sinusoidal perturbation regions were of wavelength $\lambda = 550$ μm, and the amplitude η_0 and wavenumber $k = 2\pi/\lambda$ products were $\eta_0 k \in \{1/4, 3/8, 1/2, 5/8, 3/4\}$. This $\eta_0 k$ product was chosen because it overlaps in the region of our FY10 and FY11 strength experiments, which implies that on first shock we get more Cu strength validation data, but it also implies that we can approximate the initial conditions of the surface at the arrival of the second shock. This can be considered in the context of the discussion in the preceding section. That is, some of the perturbations begin to grow plastically and the growth will arrest. This behavior has been noted in FY10 results, and seen in the FY11 results on Cu strength, and is seen in this two wave result as well.

The velocimetry in Fig. 7 shows an initial jump velocity in the flat regions of $u_{1st} \approx 1.8$ mm/μs, which correlates with $P_{SB} \approx 35$ GPa. The second shock arrives about 2.6 μs later, with a magnitude of $u_{2nd} \approx 0.9$ mm/μs. Given that the Cu is solid on first and second shock, the second shock pressure is nominally $P_{2nd} \approx 18$ GPa. This peak stress with the solid Cu is not enough to create large amounts of ejecta, as evidenced in Fig. 7 – it is not a large shock and the material remains solid. In fact, probe 3 shows that the perturbation heights grew and arrested on first shock, and that the now larger perturbations grew and arrested on second shock as well. A more complete analysis will characterize the perturbation heights at the arrival of the 2nd shock, and the perturbation heights after the arrest of the growth after the 2nd shock. But, from our FY10 experiments we can say that it is likely that the $\eta_0 k$ grew from an initial amplitude of $\eta_0 = 31$ μm to 160 μm; this would be the nominal height at the arrival of the second shock.

IV. SUMMARY

In FY11 we developed a physics based ejecta model with the FY10 campaign one data. We also used the FY10 Cu strength data to estimate the yield stress of Cu at high strains (> 700%) and high strain rates ($\varepsilon > 10^7$/s) – at zero pressure. This work set the stage for FY11 work in transport, further strength studies, and our first uniaxial strain two-shockwave experiments on Cu. The possibilities to explore with this tool are broad, but in FY12 we intend to seek a lower first shock stress so that we can field the two-wave package on Sn. The goal would be for the Sn to release to solid, but in a thermodynamic state that is just below a liquid release state. It is also of interest to shock Sn to a liquid release state and then shock it again.

We also plan to follow the first Sn-transport experiment with its companion experiments: an identical experiment into 10 Atm. He.

We acknowledge the support of the pRad team to acquire these data, especially B. Hollander, K. Kwiatkowski, M. Marr-Lyon, F. E. Merrill, P. Nedrow, A. Saunders, and W. S. Vogan-McNeil. In addition, we appreciate contributions to these experiments by members of the LANL MST-7 group where our Sn and Cu targets were machined and characterized by John Martinez and Derek Schmidt.

William T. Buttler thanks G. Dimonte and B. J. Balakumar for helpful discussions on the topics of instability physics. Also appreciated are provision of materials by G. (Rusty) T. Gray, as well as discussion of materials, material strength, and constitutive properties at high strains and strain rates.

---

[1] Buttler, W. T., Zellner, M. B., Olson, R. T., Rigg, P. A., Hixson, R. S., Hammerberg, J. E., Obst, A. W., Payton, J. R., Iverson, A. & Young, J. 2007a Dynamic comparisons of piezoelectric ejecta diagnostics. *J. Appl. Phys.* **101**, 063547.

[2] Buttler, W. T., Routley, N., Hixson, R. S., King, N. S. P., Olson, R. T., Rigg, P. A., Rimmer, A. & Zellner, M. B. 2007b Method to separate and determine the amount of ejecta produced in a second material-fragmentation event. *Appl. Phys. Lett.* **90**, 151921.

[3] Buttler, W. T. & Zellner, M. B. 2007 Tin ejecta data review: toward a statistical material fragmentation model, Milestone 2478. *Tech. Rep.* LA-UR-07-6522. Los Alamos National Laboratory.

[4] Vogan, W. S., Anderson, W. W., Grover, M., Hammerberg, J. E., King, N. S. P., Lamoreaux, S. K., Macrum, G., Morley, K. B., Rigg, P. A., Stevens, G. D., Turley, D., Veeser, L. R. & Buttler, W. T. 2005 Piezoelectric characterization of ejecta from shocked tin surfaces. *J. Appl. Phys.* **98**, 113508.

[5] Zellner, M. B., Grover, M., Hammerberg, J. E., Hixson, R. S., Iverson, A. J., Macrum, G. S., Morley, K. B., Obst, A. W., Olson, R. T., Payton, J. R., Rigg, P. A., Routley, N., Stevens, G. D., Turley, W. D., Veeser, L. & Buttler, W. T. 2007 Effects of shock breakout pressure on ejection of material from shocked tin surfaces. *J. Appl. Phys.* **102**, 013522.

[6] Zellner, M. B., Vogan-McNeil, W., Gray, G. T., III, Huerta, D. C., King, N. S. P., Neal, G. E., Valentine, S. J., Payton, J. R., Rubin, J., Stevens, G. D., Turley, W. D., & Buttler, W. T. 2008 Surface preparation methods to enhance dynamic surface property measurements of shocked metal surfaces. *J. Appl. Phys.* **103**, 083521.

[7] Zellner, M. B., Grover, M., Hammerberg, J. E., Hixson, R. S., Iverson, A. J., Macrum, G. S., Morley, K. B., Obst, A. W., Olson, R. T., Payton, J. R., Rigg, P. A., Routley, N., Stevens, G. D., Turley, W. D., Veeser, L. & Buttler, W. T. 2008 Erratum: Effects of shock-breakout pressure on ejection of material from shocked tin surfaces [(2007) *J. Appl. Phys.* **102**, 013522]. *J. Appl. Phys.* **103**, 109901.

[8] Zellner, M. B., Vogan-McNeil, W., Hammerberg, J. E., Hixson, R. S., Obst, A. W., Olson, R. T., Payton, J. R., Rigg, P. A., Routley, N., Stevens, G. D., Turley, W. D., Veeser, L. & Buttler, W. T. 2008 Probing the underlying physics of ejecta production from shocked Sn samples. *J. Appl. Phys.* **103**, 123502.

[9] Zellner, M. B. & Buttler, W. T. 2008 Exploring Richtmyer-Meshkov instability phenomena and ejecta cloud physics. *Appl. Phys. Lett.* **93**, 114102.

[10] Buttler, W. T., Lamoreaux, S. K., Omenetto, F. G. & Torgerson, J. R. 2004 Optical velocimetry. arXiv:physics/0409073v1.

[11] Forman, Jr., J. W., George, E. W. & Lewis, R. D. 1965 Feasibility study of a laser flowmeter for local velocity measurements in gas flow fields. *Tech. Rep.* Tech. Note #149, Teledyne Brown Engineering Co. Inc., Huntsville, AL.

[12] Forman, Jr., J. W., George, E. W. & Lewis, R. D. 1965 Measurement of localized fluid flow velocities in gasses with a laser Doppler flowmeter. *Appl. Phys. Lett.* **7**, 77–78.

[13] Strand, O. T., Goosman, D. R., Martinez, C. & Whitworth, R. L. 2006 Compact system for high-speed velocimetry using heterodyne techniques. *Rev. Sci. Instrum.* **77**, 083108.

[14] Yeh, Y. & Cummins, H. Z. 1964 Localized fluid flow measurements with an He-Ne laser. *App. Phys. Lett.* **4**, 176–178.

[15] Richtmyer, R. D. 1960 Taylor instability in shock acceleration of compressible fluids. *Commun. Pure Appl. Math* **13**, 297–319.

[16] Mikaelian, K. O. 1998 Analytical approach to nonlinear Rayleigh-Taylor and Richtmyer-Meshkov instabilities. *Phys. Rev. Lett.* **80**, 508–511.

[17] Zhang, Q. 1998 Analytical solution of Layzer-type approach to unsatable interfacial fluid mixing. *Phys. Rev. Lett.* **81**, 3391–3394.

[18] Mikaelian, K. O. 2010 Analytical approach to nonlinear hydrodynamic instabilities driven by time-dependent accelerations. *Phys. Rev. E* **81**, 016325.

[19] Meyer, K. A. & Blewett, P. J. 1972 Numerical investigation of the stability of a shock-accelerated interface between two fluids. *Phys. Fluids* **15**, 753–759.

[20] Velikovich, A. L. & Dimonte, G. 1996 Nonlinear perturbation theory of the incompressible Richtmyer-Meshkov instability. *Phys. Rev. Lett.* **76**, 3112–3115.

[21] Dimonte, G. & Ramaprabhu, R. 2010 Simulations and model of the nonlinear Richtmyer-Meshkov instability. *Phys. Fluids* **22**, 014104.

[22] Piriz, A. R., Lopez-Cela, J. J., Tahir, N. A., & Hoffmann, D. H. H. 2008 Richtmyer-Meshkov instability in elastic-plastic media. *Phys. Rev. E* **78**, 056401.

[23] Piriz, A. R., Lopez-Cela, J. J. & Tahir, N. A. 2009 Richtmyer-Meshkov instability as a tool for evaluating material strength under extreme conditions. *Nucl. Instrum. Meth. Phys. Res. A* **606**, 139–141.

[24] Buttler, W. T., Oró, D. M., Preston, D. L., Mikaelian, K. O., Cherne, F. J., Hixson, R. S., Mariam, F. G., Morris, C., Stone, J. B., Terrones, G. & Tupa, D., Submitted to J. Fluid Mech. (2011).

[25] Buttler, W. T., Oró, D. M., Preston, D. L., Mikaelian, K. O., Cherne, F. J., Hixson, R. S., Mariam, F. G., Morris, C., Stone, J. B., Terrones, G. & Tupa, D., Accepted for publication in AIP Shock Compression of Condensed Matter Conf. Proc. (2011).

[26] Dimonte, G., Terrones, G., Cherne, F. J., Germann, T. C., Dupont, V., Kadau, K., Buttler, W. T., Oró, D. M., Morris, C. & Preston, D. L., "Use of Richtmyer-Meshkov instability to infer yield stress at high-energy-density," Submitted to Phys. Rev. Lett. (2011).

[27] Bourne, N. K. & Gray, G. T., III 2005a Computational design of recovery experiments for ductile materials. *Proc. Royal Soc. A* **461**, 3297–3313.

[28] Bourne, N. K. & Gray, G. T., III. 2005b Soft-recovery of shocked polymers and composites. *J. Phys. D: Appl. Phys.* **38**, 3690–3694.